Computational design of magnetic beamlet deflection correction for NNBI

Niek den Harder,[a] Guillermo Orozco, Riccardo Nocentini, Bernd Heinemann, Andrew Hurlbatt, Federica Bonomo, and Ursel Fantz
Max-Planck-Institut für Plasmaphysik, Garching bei München, Germany
Pierluigi Veltri
ITER Organization, Saint-Paul-lez-Durance, France

Coextracted electrons are inevitable for negative ion based NBI systems. To avoid wastefully accelerating these electrons to the full energy, they are magnetically deflected out of the beamlet onto the extraction grid. The deflection of the electrons creates an unwanted deflection of the ions, which is magnetically corrected in the ITER heating neutral beam. In order to gain experience with magnetic deflection correction, IPP has designed a magnetic deflection correction system in collaboration with the ITER organization, which will be characterized in the BATMAN Upgrade test facility. The ion-optics code IBSimu is used for the design of the magnetic deflection correction system. A comparison of the design candidates shows that the magnetic deflection correction system inherently leads to an increased divergence as result of the magnetic field structure. The divergence increase manifests itself as an increased fraction of a broader halo component.

I. INTRODUCTION

Neutral Beam Injection (NBI) will be the main heating system of ITER. The Heating Neutral Beams (HNB) are designed to deliver 33 MW to the plasma by 2 injectors that accelerate negative hydrogen/deuterium ions to 1 MeV by means of a 7 grid system from 1280 apertures[1]. The ITER NBI system is based on negative ions since the neutralization efficiency of positive ion beams is vanishingly small at energies above 100 keV/amu[2,3]. The negative ions are generated in an RF-driven plasma source, mostly on the plasma facing surfaces by conversion of atoms and positive ions[4]. The negative ions are extracted from the quasineutral plasma by the extraction potential of approximately 10 kV, applied between the plasma facing grid (plasma grid) and the following downstream grid (extraction grid). After extraction, the negative ions are accelerated to the full energy in 5 acceleration steps. There are strict requirements on the source operating parameters and beamlet properties.

The ITER NBI plasma source should operate at filling pressures below 0.3 Pa. Due to stripping losses in the grid system, it is necessary to homogeneously ($\pm$ 10%) extract current densities of 329 A/m^2 in hydrogen, and 286 A/m^2 in deuterium with a pulse length of 1000 s in H and 3600 s in D[1,5,6]. The ITER beamlines are designed assuming a double Gaussian profile for the angular distribution of the beamlets with a core carrying 85 % of the power at a divergence in the range 3-7 mrad, and a halo at a divergence of 15-30 mrad[1,7]. A beamlet misalignment of 2 mrad in the horizontal, and 4 mrad in the vertical direction is considered as worst case scenario that still meets the ITER requirements[1,7]. The whole source can be tilted by $\pm$10 mrad from the nominal downward inclination of 49.2 mrad to correct a net vertical angle of the beam[7].

[a]Electronic mail: niek.den.harder@ipp.mpg.de

Coextracted electrons are inevitable for negative ion based NBI systems. A filter field on the order of a few mT in the extraction region magnetizes the electrons but not the ions, and reduces both the electron temperature and density in front of the plasma grid[8]. This improves the coextracted electron-to-ion ratio, which should be smaller than one, by suppressing negative ion destruction and reducing the amount of electrons that are available to be extracted[9]. To avoid wastefully accelerating the coextracted electrons to full energy, they are deflected onto the extraction grid in the extraction gap. The horizontal deflection of the electrons is caused by a vertical magnetic field which alternates direction row-wise, created by permanent magnets embedded in the extraction grid. These permanent deflection magnets are called CESM (Co-extracted Electron Suppression Magnets). The alternating magnetic field also creates an unwanted row-wise zig-zag deflection of the ions, which should be corrected in order to satisfy the beamlet misalignment requirements.

The beamlet angles can be corrected electrostatically or magnetically. Earlier ITER-HNB designs relied on electrostatic correction, by aperture offset steering[10,11]. The most recent ITER-HNB design magnetically corrects the beamlet angles, which, unlike electrostatic compensation, does not depend on the total energy[12]. In the pure magnetic deflection model, the beamlet angle simply depends on the integral of the vertical magnetic field along the beamlet axis[13]. This integral is nonzero since the beamlet particles are collisional inside the plasma, and the lower limit of the integral should be placed at the location where collisional properties become negligible and particles start following paths defined by the Lorentz force. In the ITER-HNB grid design, magnetic deflection correction is achieved by strengthening the magnetic field upstream of the extraction grid with a second set of magnets which, together with the deflection magnets, form a one-sided magnetic flux structure[12,14,15]. These permanent correction magnets are called ADCM (Asymmetric Deflection Compensation Magnets), which were first introduced in References[16,17]. Figure 3 shows an exam-

ple of an extraction grid with an embedded magnet array seen from the downstream, i.e. the field weakening side. The magnetic field needed to correct the deflection also depends on the electric field, since both the applied electrode potentials and the space charge induced deformation of the electrostatical lenses factor into the final deflection[13].

In the framework of a research collaboration between Consorzio RFX (Italy) and QST (Japan), magnetic deflection correction has been explored in the Negative Ion Test Stand (NITS) of QST with a single aperture geometry identical to the ITER-HNB plasma grid and extraction grid. Deflection correction was demonstrated under restrictive conditions: an acceleration potential below 10 kV[18]. Since the deflection is corrected in the divergence optimum, the extraction potential was approximately 1 kV, and the current densities on the order of 10 A/m^2. A more extensive characterization of the magnetic deflection correction system is foreseen in the BATMAN Upgrade test facility (BUG), which is capable of reaching the ITER extracted current density targets and can operate in hydrogen and deuterium, but is limited to a total high-voltage of 45 kV[19]. This paper presents a benchmark of the modeling tools on the RFX-QST NITS campaigns, a design of a magnetic deflection correction system for BUG, and a computational study on the impact of magnetic deflection correction on the beamlet divergence.

II. COMPUTATIONAL METHODS

Single aperture magnetic fields are calculated with ANSYS, which takes into account the magnet-magnet interaction. ANSYS is also used to calculate the filter field that is generated by a current through the plasma grid. Whole grid magnetic fields including edge effects, are calculated with the in-house developed BioMAGPy code, which is based on an integral formulation and allows an efficient calculation of static magnetic field configurations with linear materials and permanent magnets[20].

Modeling the processes which create and destroy charged particles in the plasma from first principles is computationally expensive. A cheaper approach is to treat the negative ions explicitly by tracking them through the fields, while approximating the plasma behaviour by a model which describes the local charge density of the compensating positive ions. IBSimu is used since it is 3D, open-source, and distributed as C++ library so that it is highly customizable[21,22].

The single aperture grid geometry is implemented via analytical functions based on technical drawings of the grid systems. Grid designs have been published for both BUG[19] and the ITER-HNB[12] geometries. Negative hydrogen ions and electrons enter the full surface of the simulation box 2 mm before the plasma grid with a starting energy of 3 eV, and a parallel and perpendicular temperature of 1 eV. All the simulation particles are thus effectively from the plasma volume, although in the experiment negative ion production on caesiated surfaces is essential, and modeling indicates that the surface produced ions have a different angular distribution[23,24]. The $T_\perp$ of 1 eV is pessimistic, previous modeling studies used 0.8 eV for the neutrals and positive ions[25]. A negative ion temperature of 0.2 eV is estimated for arc sources[23]. For RF sources only a gas temperature measurement is available, which shows 54 % of the gas as a cold population of 628 K, and the remaining gas at a temperature of 4500 K near the plasma grid[26]. The current density at the injection plane J_{inj} and the potentials are varied in the simulations, the other input parameters are kept constant.

To model the modification of the electric field by the charged particles themselves, the Poisson equation is solved in an iterative scheme, including the space charge of the tracked particles. A finer solution in less CPU time is achieved by using a multigrid approach. The space charge is calculated by summing the currents of the simulation particles weighted by the time they spend in a simulation cell. In the plasma region, there are compensating charges such that the net space charge is zero. These compensating charges are not explicitly tracked, an analytical function generates the charge density of thermal positive ions whose temperature is a free user parameter. In this study 0.8 eV is used as in previous studies, the results are not very sensitive to this parameter[25]. The magnetic field is suppressed in the plasma region, which is defined as the cells where the potential is below 1 Volt. The plasma grid is always at a potential of 0 Volt in the simulations.

Coextracted electrons are negligible for the ion optics, as for an equal current density to negative ions they contribute $\sqrt{m_H/m_e} \approx 43$ times less to the space charge. A co-extracted electron fraction of 1 is the upper limit for safe operation of the BUG and ITER sources at full parameters in view of extraction grid heat loads[9]. The background gas density and associated stripping losses is not included, since it has only a small influence on the space charge.

The coextracted electrons cause the main part of the heat load on the extraction grid[27]. Power density profiles are modeled in separate simulations, which run with half a million negative ions and half a million coextracted electrons. The horizontal and vertical boundaries in these simulations are periodic, and include the row-wise reversal of magnetic field direction.

It is assumed that 10 mm after the last grid, which is grounded in the experiment (GG), space charge compensation has set in, and there is no net local charge density and associated electric field that changes the particle distribution[28].

In the context of NBI systems, the angular distribution of the beamlet is of particular interest, since it largely determines the beamline transmission. A single Gaussian

divergence is calculated from the particle angles as:

$$\theta_{1/e} = \sqrt{2\langle \arctan\left(\frac{v_y - \langle v_y \rangle}{v_x}\right)^2 \rangle} \quad (1)$$

The average velocity needs to be subtracted to get a correct value for non-centred distributions. The divergence $\theta_{1/e}$ is the angle between the beamlet axis and locations where the power density is reduced a factor $1/e$ with respect to the on-axis value. In IBSimu, the particles start with an initial perpendicular temperature, which corresponds to an initial divergence θ_T of:

$$\theta_T = \sqrt{\frac{T_\perp}{U_{\text{tot}}}} \quad (2)$$

where U_{tot} is the sum of the extraction potential U_{ext} (applied between PG and EG) and the acceleration potential U_{acc} (applied between EG and GG). This equation assumes that the initial particle distribution is accelerated to U_{tot} by an increase of the parallel velocity while the perpendicular velocity is unchanged. Because the divergence is an angle, the initial temperature contribution depends on U_{tot}.

For more insight into the shape of the angular distribution, a double Gaussian is fitted at the end of the accelerator exit: a core Gaussian with a smaller divergence, and a halo Gaussian with a larger divergence. Since the double Gaussian fit adheres to the $1/e$ definition, adding the two components geometrically recovers the single Gaussian divergence $\theta_{1/e}$. Double Gaussian distributions have been observed in experiment, several hypotheses have been proposed to explain beam halos[29]. It is known that negative ions extracted from the periphery of the plasma grid aperture tend to have a broader angular distribution[30]. Magnetic deflection and compensation lead to a non-centred traversal of the electrostatic lenses, which induces aberrations in the angular distribution. Surface production of negative ions on downstream plasma grid surfaces could lead to a halo[29]. Stripping of negative ions inside the acceleration system has been put forward as possible explanation[31]. Surface production and stripping are not included in the current simulations.

III. RESULTS

A. Benchmark of modeling tools

Magnetic correction of the beamlet deflection has been demonstrated in the test facility NITS of QST, in the framework of a research collaboration between Consorzio RFX and QST[32]. A partial discrepancy between OPERA[33] simulations and measured deflection correction was found, which was attributed to a horizontal asymmetry of the current density over a single aperture in the experiment[32]. Before a BUG magnet design is attempted, the modeling tools will be benchmarked on the published NITS measurements[32].

The NITS magnetic fields are calculated with ANSYS. The filter field is neglected because it almost exclusively impacts the vertical position of the beam. IBSimu single aperture beamlet calculations are performed, beamlet-beamlet interaction is neglected. The particles are projected in straight lines from the end of the simulation domain, which is 10 mm downstream of the grounded grid, to the CFC, which is 94 cm from the GG[32]. The beamlets are cloned to the known aperture positions.

Figure 1 shows a calculated CFC power density profile for discharge 10574 of the RFX-QST NITS campaign. The CESM magnets have a remanence of 1.1 T, and the ADCM magnets have a remanence of 0.88 T, which corresponds to the initial design[32]. During the NITS experiments, the ADCM magnets were only present in the lower grid half. For each aperture, the average of the particle positions at the CFC location is calculated to define the beamlet position, which is indicated by the gray circles. The average position can deviate from the peak power density, for example due to a variation of the vertical width in the horizontal direction. This effect is more pronounced close to the grid system, at low U_{tot}, and at low $T_\perp$. The measured profiles appear sharper even after heat transfer in the CFC, indicating that the perpendicular temperature of 1 eV is a pessimistic assumption for the considered case. There is reasonable agreement between the calculated and measured horizontal beamlet positions shown in Reference[32] (Figure 9) without including a current density asymmetry in the modeling. The differences between the OPERA and IBSimu simulations are likely due to a different implementation of the plasma model. Because the filter field is neglected, the calculated vertical position of the beamlets does not match the measurements[34]. Since the modeled horizontal positions agree reasonably with the measured positions without the need for a correction factor, the applied tools can be used for the design of the BUG-MLE.

B. BUG-MLE Magnet design

In order to perform experiments with a magnetic deflection correction system in BUG, the test facility will be equipped with the ITER-HNB plasma grid and extraction grid geometry, and the standard BUG grounded grid. The extraction gap of 6 mm is kept identical to the ITER-HNB design[12]. The acceleration gap is set to 12 mm, since this leads to an almost identical modeled optimum $U_{\text{acc}}/U_{\text{ext}}$ ratio as the standard BUG configuration, which has an acceleration gap of 15 mm. In addition, the 12 mm acceleration gap reproduces the proof-of-principle demonstration of the deflection correction system in NITS[32]. The configuration with the ITER-HNB plasma grid and extraction grid is called MITICA-Like Extraction (MLE). MITICA is the full prototype injector of the ITER-HNB[35]. Figure 2 shows the standard BUG grid configuration together with the new grid system.

Calculations are reported for the divergence optimum

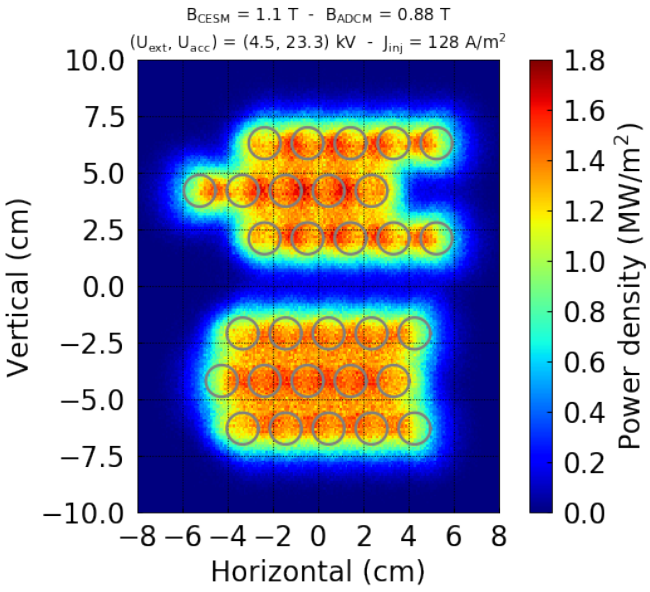

FIG. 1: Calculated CFC power density profile for discharge 10574 of the RFX-QST NITS campaign by projecting the IBSimu particles[32]. Grey circles indicate the beamlet centers.

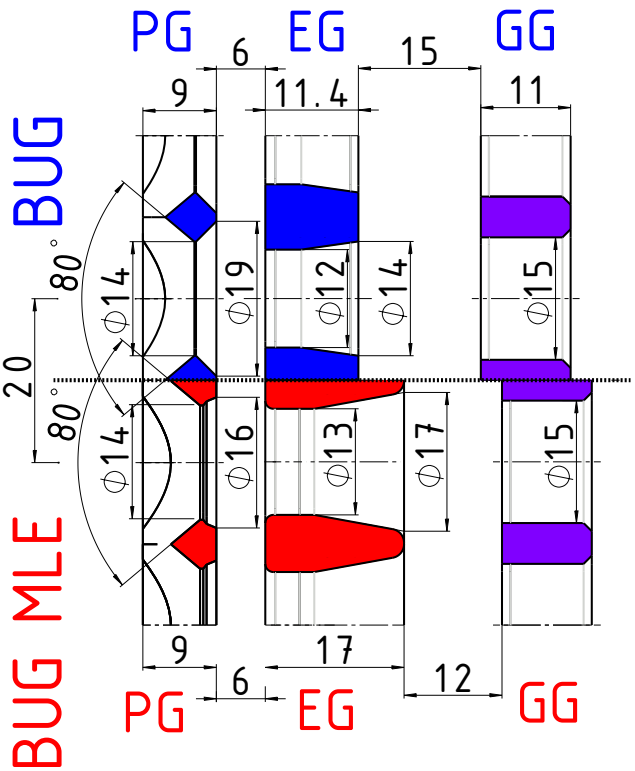

FIG. 2: The standard BUG plasma grid (PG), extraction grid (EG), and grounded grid (GG) shown in blue, together with the BUG MITICA-Like Extraction grid system (red).

at an extraction potential of 5 kV and an acceleration potential of 26 kV. The simulations are below the experimental 45 kV limit, to provide buffer to scan around the optimum in the experiment. Standard BUG has a horizontal beamlet deflection of 11 mrad in these conditions. In the BUG-MLE configuration, the deflection should be corrected in the divergence optimum. The magnetic deflection correction does not depend on the total beam energy[13].

Because the standard BUG grounded grid is used, the distance between apertures is 20 x 20 mm (horizontal x vertical). This is different from the 19 x 21 mm in NITS[32], and the 20 x 22 mm in the ITER-DNB and HNB[7,36]. The different aperture spacing in BUG with respect to the NITS configuration is one of the reasons the magnet design from NITS is not directly transferable to BUG.

Magnetic deflection correction depends on the ratio of the magnetic field strength upstream and downstream of the extraction grid; the absolute field strength upstream of the extraction grid is in principle a free parameter in the magnet design. There is a minimum field strength required to dump the electrons on the upstream surface of the extraction grid, which is between 40 and 50 mT for the BUG-MLE geometry at 10 kV extraction potential: the most demanding condition in terms of coextracted electrons. The magnet design is based on VACOMAX 225 HR, the Sm_2Co_{17} material used for the deflection magnets in BUG and other IPP test facilities. Because the ADCM magnets strengthen the field upstream of the extraction grid, keeping the standard BUG CESM magnet size and adding the ADCM magnets will result in a higher peak vertical field than the standard on-axis value of 62 mT. The RFX-QST NITS 2017 campaign that demonstrated complete deflection correction had low peak field strengths of 46 mT[18]. For the BUG-MLE design, it is chosen to imitate the standard BUG magnetic field. This results in a reduced CESM size of 20 x 3.4 x 6.8 mm (width x height x depth), so that BUG-MLE with ADCM magnets has a comparable peak field strength upstream of the extraction grid compared to the standard BUG, which has 20 x 5 x 6 mm CESM size. The width is the size in horizontal direction, the height is the size in the vertical direction, and the depth is the size in the axial direction.

In the RFX-QST NITS design, the CESM and ADCM magnets have the same depth, resulting in very thin ADCM magnets. This is a design choice, several ADCM shapes can be used to correct the deflection, although the magnet volume varies slightly since the field topology changes with the magnet shape. For BUG-MLE, it was chosen to have 2 x 16.2 x 4 mm ADCM magnets, since these are more robust mechanically. Additionally, the grid manufacturing process is easier since the magnet grooves have a more symmetrical aspect ratio. Figure 3 shows the extraction grid seen from downstream, i.e. the field weakening side. Small vertical correction magnets in between the horizontal deflection magnets form an asym-

metric magnetic flux structure. Because the polarity of the correction magnets aligns with the deflection magnets, the correction magnets are repelling the deflection magnets, which is a safeguard to ensure correct assembly. The position of the ADCM magnets can be inspected with 6 mm diameter holes on the downstream side of the extraction grid. Figure 4 shows the vertical magnetic field component for the NITS 2017 configuration, the standard BUG configuration, and BUG-MLE with and without ADCM. In the BUG-MLE configuration with ADCM, the integral of the vertical field upstream of the magnets is 1.8 times the downstream vertical field integral.

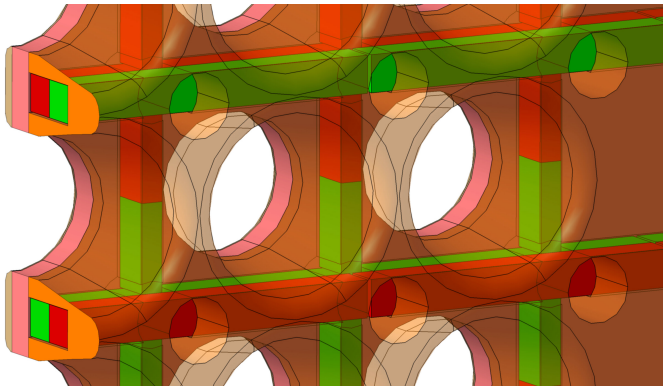

FIG. 3: Small vertical correction magnets in between the horizontal deflection magnets form a Halbach array: an asymmetric magnetic flux structure. The extraction grid is seen from the downstream, i.e. field weakening side. Cooling channels not shown; grid colours show manufacturing steps by electrodeposition.

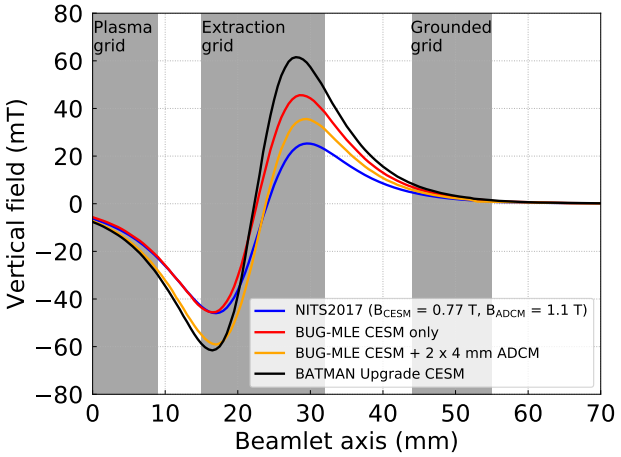

FIG. 4: The on-axis vertical magnetic field for various experimental configurations. The BUG-MLE grids are indicated by grey blocks.

Both the magnet material properties and the magnet shape have tolerances after manufacturing. The VACOMAX 225 HR material has a catalogue remanence of 1.1 T and coercivity of 820 kA/m, with minimum values of 1.03 T for the remanence and 720 kA/m for the coercivity[37]. Machining tolerances are 0.1 mm at most. The impact of expected variations in the magnetic properties and machining tolerances of the magnets was investigated by randomly varying the magnet properties for a number of apertures. For the BUG-MLE magnetic design, in the divergence optimum at 5 kV extraction potential, this leads to a variation of the beamlet angle with a bandwidth of 0.4 mrad for the catalogue range of magnetic properties and the 0.1 mm size variation, which is acceptable.

Electrostatic multibeamlet effects were explored to assess the impact of beamlet-beamlet repulsion on the beamlet angle. During extraction and acceleration, the beamlets are negatively charged and repel each other. After the grid system, the space charge of the beamlet is compensated by positively ionized background gas attracted by the negative potential well. The beamlet repulsion can be compensated by aperture offset (SPIDER[38]), or by kerbs (ITER-DNB[36], ITER-HNB[12]). For BUG-MLE, the beamlet-beamlet repulsion is small, roughly 1 mrad at 5 kV U_{ext} and 26 kV U_{acc}. At the downstream side of the extraction grid, the edge beamlets do not have neighbouring apertures. This asymmetric geometry deforms the potential in a similar way intentionally placed kerbs would; the beamlets deflect inward as a result. The inward geometric deflection is stronger than the outward beamlet-beamlet repulsion, leading to a net inward angle of the edge beamlets. In the presence of magnetic fields, the beamlets are off-center throughout most of the grid system, and asymmetric kerbs are needed to correct the beamlet-beamlet repulsion. Since the beamlet-beamlet repulsion angle is small, and the correction is too complex to implement with respect to the expected outcome, the design does not include kerbs.

Magnetic edge effects were explored to translate the single aperture magnet design to a full grid design. The ANSYS magnetic field calculations are performed assuming periodic boundary conditions, and thus correspond to an infinitely large grid. In the experiment, the outer apertures have a slightly different magnetic field due to edge effects. Full grid magnetic fields were calculated with the BioMAGPy code[20]. The most basic BUG-MLE implementation surrounds every single aperture with magnets. The CESM magnets are as wide as used in the standard BUG configuration. The beamlet angles are studied in the divergence optimum at U_{ext} of 5 kV, U_{acc} of 26 kV, and J_{inj} of 150 A/m^2. The minimal implementation of BUG-MLE is fine for the beamlets at the horizontal edges, which are within 0.4 mrad of the horizontally central beamlet angle, thus extra ADCM magnets at the sides are not necessary. The angles of the vertically outermost beamlets deviate more, because the ADCM magnets do not lead to such an asymmetric flux structure as for the central apertures. To equalize the

magnetic field for the outer apertures, an extra row of CESM and ADCM is mounted at the top and bottom of the grid. This decreases the standard deviation of the horizontal beamlet angles in the vertically central, next to outermost, and outermost beamlets from 2.2 mrad to 1 mrad.

C. Impact of deflection correction on divergence

The magnet dimensions reported in Section III B are the result of an extensive design process, many different permanent magnet configurations compatible with the BUG-MLE grid geometry were studied. In this section, the database of modeled magnetic fields and corresponding IBSimu simulations is used to analyze whether the simulated divergence can be linked to key magnetic field parameters.

Figure 5 shows the horizontal and vertical divergence for the BUG-MLE geometry as function of the peak on-axis vertical magnetic field strength. As in the previous section, the values are given in the divergence optimum of 5 kV U_{ext}, 26 kV U_{acc}, and 150 A/m^2 J_{inj}. Not all configurations are viable candidates, low field strength configurations are added to cover the x-axis. Only compensated configurations with an absolute beamlet angle of less than 2 mrad, measured 10 mm after the grounded grid, are shown. The peak field strength is a crucial parameter: at increased vertical magnetic field strength, the divergence increases. At stronger vertical magnetic fields, the beamlet is further displaced horizontally from the aperture axis. The offset from the aperture center induces distortions in the horizontal and vertical angular distribution. The distortions only become noticeable at high field strengths, there is a quadratic peak field strength dependence. The configurations with ADCM magnets have a higher vertical divergence, an effect not seen for configurations which only have CESM magnets. The aspect ratio of the ADCM magnets, i.e. whether the cross section is rectangular or square, has no significant impact on the divergence for the studied configurations.

The divergence increase due to the magnetic fields is visible in the angular distribution as an increase in the halo fraction and the halo divergence. As shown in Figure 5, the horizontal and vertical core divergence are almost identical, and only increase weakly with the magnetic field strength. The increase in the halo fraction causes the main part of the divergence increase.

The higher vertical divergence for configurations with ADCM is caused by the magnetic field structure. Figure 6 shows the BUG-MLE magnetic field structure on a plane perpendicular to the beamlet direction, at an axial location close to the center of the ADCM magnets, seen from the upstream side looking in the downstream direction. The grid aperture is indicated by a white circle surrounded with the area in grey; the CESM and ADCM magnets are shown in red/blue. The ADCM magnets add a horizontal component to the magnetic

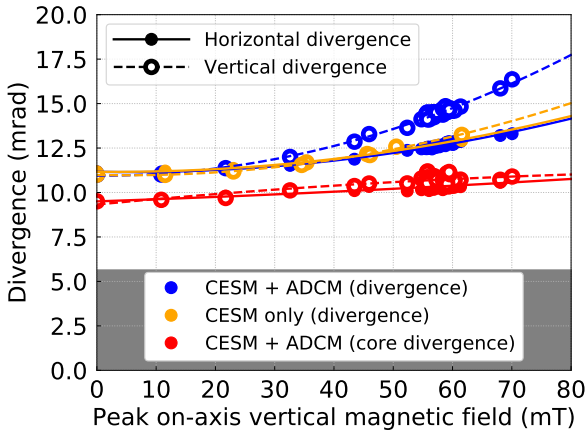

FIG. 5: Horizontal and vertical divergence in BUG-MLE geometry for several magnetic field configurations as function of the peak on-axis vertical magnetic field strength. Gray shading indicates the $T_\perp$ contribution of 1 eV. Values given for the divergence optimum of 5 kV U_{ext}, 26 kV U_{acc}, and 150 A/m^2 J_{inj}.

field, which is small compared to the vertical field generated by the larger CESM magnets. The vertical field component leads to a displacement of the beamlet from the aperture center; the Lorentz force pushes the beamlet towards the right side of the aperture in the extraction grid. The horizontal field component causes a downward force in the lower left and upper right quadrant, and an upward force in the upper left and lower right quadrant, i.e. the horizontal field component defocuses the left side of the beamlet, and focuses the right side of the beamlet. The vertical deflection field changes sign, but the ADCM horizontal field components have the same direction upstream and downstream of the magnets. Although the horizontal magnetic field component generated by the ADCM is partially focusing, the net effect is a broadening of the angular distribution.

To demonstrate that the horizontal magnetic field component generated by the ADCM increases the vertical divergence, the BUG-MLE configuration was modeled with the horizontal magnetic field component set to zero. This is unphysical since the ADCM magnets produce a horizontal field, and is only intended to show the effect of this component on the ion-optics. Without horizontal magnetic field component, the horizontal and vertical divergence are approximately equal, i.e. no increased vertical divergence.

The influence of the filter field was simulated for the BUG-MLE configuration for a typical plasma grid current of 1.5 kA which generates a field of 5 mT[39]. The filter field has negligible impact on the divergence since it has the same direction over the aperture, so that it only causes a vertical deflection.

To illustrate the effect of the ADCM on the beamlet

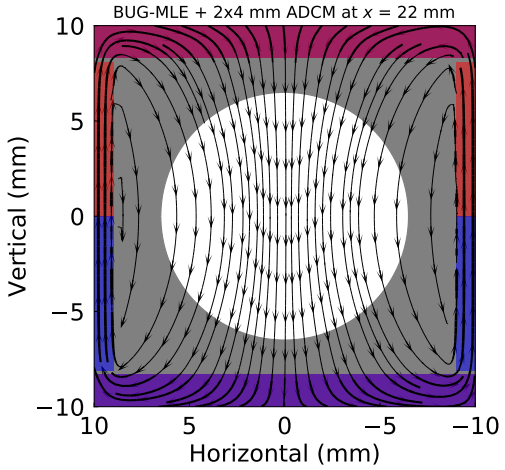

FIG. 6: A schematic of the magnetic field geometry close to the center of the ADCM magnets seen from the upstream side looking downstream. The horizontal field component leads to a vertical defocusing on the left and a focusing on the right side of the beamlet.

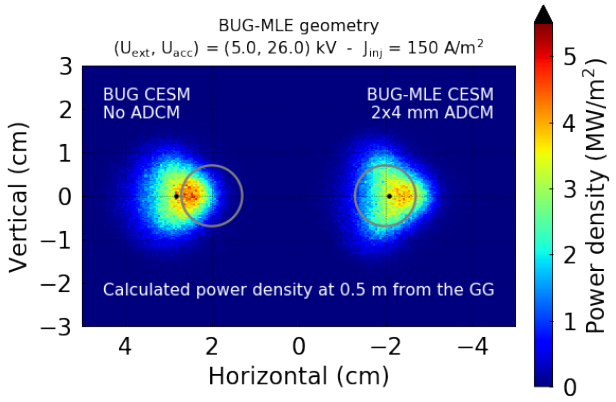

FIG. 7: A side-by-side comparison of the power density 0.5 m downstream of the GG for the BUG-MLE geometry, but with the BUG CESM (left) and BUG-MLE CESM + 2x4 mm ADCM (right), which have an almost identical peak field. The grey circles show aperture positions, black dots beamlet centers.

shape, Figure 7 shows the power density 0.5 m from the grounded grid for the BUG-MLE geometry with the BUG CESM (left) and BUG-MLE CESM + 2x4 mm ADCM (right). Both magnetic configurations have a similar peak vertical field strength. With and without ADCM, the beamlet is vertically compressed at the side where the beamlet gets close to the extraction grid. The ADCM horizontal magnetic field component additionally focuses the beamlet vertically at the this side, and defocuses on the other side, a small but systematic effect that leads to a higher vertical divergence. Because of the variation in vertical width, the average horizontal location does not coincide with the peak power density.

At higher extraction potential, the impact of the magnetic field on the particle angles and positions is smaller. In MITICA and the ITER-HNB, the planned electron deflection field strength is 60 mT[40]. For the simulations shown in Figure 5, the horizontal and vertical divergences are increased by 14 % and 35 % respectively, at 60 mT compared to the value at 0 mT. The comparison is made to an unrealistic field strength of 0 mT, since this gives the impact of the magnetic field compared to the field-free case. At 10 kV extraction potential, the horizontal and vertical divergences are increased by 8 % and 23 % respectively, at 60 mT compared to the value at 0 mT. Still, it is difficult to extrapolate these results; MITICA and the ITER-HNB accelerate the particles to 1 MeV, and have additional secondary electron suppression magnets installed in the acceleration grids.

IV. CONCLUSIONS

IPP has designed a magnetic deflection correction system in collaboration with the ITER organization, which will be tested in the BUG test facility. The system is designed for a single aperture grid geometry with the ITER-HNB plasma grid and extraction grid, and the standard BUG grounded grid, which will be referred to as the BUG-MLE geometry. The modeling tools used for the design were benchmarked on the RFX-QST NITS campaigns. The BUG-MLE geometry is chosen to have a 6 mm extraction gap and 12 mm acceleration gap, to reproduce the geometry used in the RFX-QST NITS campaigns. The magnetic deflection correction is designed to have a magnetic field upstream of the extraction grid which is close to the standard BUG magnetic field. This results in a CESM size of 20 x 3.4 x 6.8 mm (width x height x depth), whereas the standard BUG configuration has a CESM size of 20 x 5 x 6 mm. The ADCM magnets are 2 x 16.2 x 4 mm. The rectangular cross section was chosen for mechanical robustness, and it makes the extraction grid easier to manufacture. The database of configurations generated in the design process was studied to quantify the impact of the magnetic fields on the divergence. At increased vertical magnetic field strength, the divergence increases. The configurations with ADCM magnets have a higher vertical divergence, an effect not seen for configurations which only have CESM magnets. The increased vertical divergence is linked to the horizontal magnetic field component generated by the ADCM magnets. The divergence increase manifests itself as an increased fraction of a broader halo component. The impact of magnetic deflection correction on the vertical divergence and ultimately beamline transmission, especially in comparison with electrostatic compensation, should be further studied.

The plasma grid insert and extraction grid are manufactured. An extensive characterization of the grid with a spectrum of diagnostics is planned to be completed in 2021.

V. ACKNOWLEDGMENTS

This work has been carried out within the framework of the EUROfusion Consortium and has received funding from the Euratom research and training programme 2014-2018 and 2019-2020 under grant agreement No 633053. The views and opinions expressed herein do not necessarily reflect those of the European Commission.

The views and opinions expressed herein do not necessarily reflect those of the ITER Organization.

[1] INTERNATIONAL ATOMIC ENERGY AGENCY, *ITER Technical Basis*, ITER EDA Documentation Series No. 24 (INTERNATIONAL ATOMIC ENERGY AGENCY, Vienna, 2002).

[2] S. K. Allison, Review of Modern Physics **30**, 1137 (1958).

[3] K. H. Berkner, R. V. Pyle, and J. W. Stearns, Nuclear Fusion **15**, 249 (1975).

[4] M. Bacal and M. Wada, Applied Physics Reviews **2**, 021305 (2015), https://doi.org/10.1063/1.4921298.

[5] R. Hemsworth, H. Decamps, J. Graceffa, B. Schunke, M. Tanaka, M. Dremel, A. Tanga, H. D. Esch, F. Geli, J. Milnes, T. Inoue, D. Marcuzzi, P. Sonato, and P. Zaccaria, Nuclear Fusion **49**, 045006 (2009).

[6] A. Krylov and R. Hemsworth, Fusion Engineering and Design **81**, 2239 (2006).

[7] R. Hemsworth, D. Boilson, P. Blatchford, M. D. Palma, G. Chitarin, H. de Esch, F. Geli, M. Dremel, J. Graceffa, D. Marcuzzi, G. Serianni, D. Shah, M. Singh, M. Urbani, and P. Zaccaria, New Journal of Physics **19**, 025005 (2017).

[8] S. Lishev, A. Shivarova, and K. H. Tarnev, Journal of Physics: Conference Series **223**, 012003 (2010).

[9] R. Hemsworth, A. Tanga, and V. Antoni, Review of Scientific Instruments **79**, 02C109 (2008), https://aip.scitation.org/doi/pdf/10.1063/1.2814248.

[10] H. de Esch, M. Kashiwagi, T. Inoue, G. Serianni, P. Agostinetti, G. Chitarin, N. Marconato, E. Sartori, P. Sonato, P. Veltri, and R. Hemsworth, AIP Conference Proceedings **1515**, 512 (2013), https://aip.scitation.org/doi/pdf/10.1063/1.4792823.

[11] M. Kashiwagi, M. Taniguchi, N. Umeda, M. Dairaku, H. Tobari, H. Yamanaka, K. Watanabe, T. Inoue, H. de Esch, L. Grisham, D. Boilson, R. Hemsworth, and M. Tanaka, AIP Conference Proceedings **1515**, 227 (2013), https://aip.scitation.org/doi/pdf/10.1063/1.4792789.

[12] H. de Esch, M. Kashiwagi, M. Taniguchi, T. Inoue, G. Serianni, P. Agostinetti, G. Chitarin, N. Marconato, E. Sartori, P. Sonato, P. Veltri, N. Pilan, D. Aprile, N. Fonnesu, V. Antoni, M. Singh, R. Hemsworth, and M. Cavenago, Nuclear Fusion **55**, 096001 (2015).

[13] M. Cavenago and P. Veltri, Plasma Sources Science and Technology **23**, 065024 (2014).

[14] J. Mallinson, IEEE Transactions on Magnetics **9**, 678 (1973).

[15] K. Halbach, Nuclear Instruments and Methods **169**, 1 (1980).

[16] G. Chitarin, P. Agostinetti, D. Aprile, N. Marconato, and P. Veltri, Review of Scientific Instruments **85**, 02B317 (2014), https://doi.org/10.1063/1.4826581.

[17] G. Chitarin, "MAGNET GRID," (2014), patent WO/2014/191890.

[18] G. Chitarin, A. Kojima, D. Aprile, P. Agostinetti, M. Barbisan, S. Denizeau, M. Ichikawa, J. Hiratsuka, M. Kashiwagi, N. Marconato, A. Pimazzoni, E. Sartori, G. Serianni, P. Veltri, and M. Yoshida, Fusion Engineering and Design **146**, 792 (2019), sI:SOFT-30.

[19] B. Heinemann, M. Fröschle, H.-D. Falter, U. Fantz, P. Franzen, W. Kraus, R. Nocentini, R. Riedl, and B. Ruf, AIP Conference Proceedings **1655**, 060003 (2015), https://aip.scitation.org/doi/pdf/10.1063/1.4916472.

[20] A. Hurlbatt, Private Communication (2020).

[21] T. Kalvas, O. Tarvainen, T. Ropponen, O. Steczkiewicz, J. Ärje, and H. Clark, Review of Scientific Instruments **81**, 02B703 (2010), https://doi.org/10.1063/1.3258608.

[22] T. Kalvas, *Development and use of computational tools for modelling negative hydrogen ion source extraction systems*, Ph.D. thesis, University of Jyväskylä (2013).

[23] R. Hemsworth and T. Inoue, IEEE Transactions on Plasma Science **33**, 1799 (2005).

[24] I. Montellano, D. Wünderlich, S. Mochalskyy, and U. Fantz, Journal of Physics D: Applied Physics **52**, 235202 (2019).

[25] D. Wünderlich, R. Gutser, and U. Fantz, Plasma Sources Science and Technology **18**, 045031 (2009).

[26] S. Briefi and U. Fantz, AIP Conference Proceedings **2052**, 040005 (2018), https://aip.scitation.org/doi/pdf/10.1063/1.5083739.

[27] R. Nocentini, R. Gutser, B. Heinemann, M. Fröschle, and R. Riedl, Fusion Engineering and Design **86**, 916 (2011), proceedings of the 26th Symposium of Fusion Technology (SOFT-26).

[28] C. Valerio-Lizarraga, I. Leon-Monzon, and R. Scrivens, Phys. Rev. ST Accel. Beams **18**, 080101 (2015).

[29] H. de Esch and L. Svensson, Fusion Engineering and Design **86**, 363 (2011).

[30] K. Miyamoto, S. Nishioka, I. Goto, A. Hatayama, M. Hanada, A. Kojima, and J. Hiratsuka, Review of Scientific Instruments **87**, 02B124 (2016), https://doi.org/10.1063/1.4932390.

[31] K. Miyamoto, Y. Fujiwara, T. Inoue, N. Miyamoto, A. Nagase, Y. Ohara, Y. Okumura, and K. Watanabe, AIP Conference Proceedings **380**, 390 (1996), https://aip.scitation.org/doi/pdf/10.1063/1.51279.

[32] G. Chitarin, A. Kojima, P. Agostinetti, D. Aprile, C. Baltador, J. Hiratsuka, M. Ichikawa, N. Marconato, E. Sartori, G. Serianni, P. Veltri, M. Yoshida, M. Kashiwagi, M. Hanada, and V. Antoni, AIP Conference Proceedings **1869**, 030026 (2017), https://aip.scitation.org/doi/pdf/10.1063/1.4995746.

[33] Vector Fields Co. Ltd, "OPERA-3D," `http://operafea.com/` (2020).

[34] D. Aprile, P. Agostinetti, C. Baltador, S. Denizeau, J. Hiratsuka, M. Ichikawa, M. Kashiwagi, A. Kojima, N. Marconato, A. Pimazzoni, E. Sartori, G. Serianni, P. Veltri, M. Yoshida, and G. Chitarin, AIP Conference Proceedings **2052**, 070001 (2018), https://aip.scitation.org/doi/pdf/10.1063/1.5083781.

[35] P. Agostinetti, D. Aprile, V. Antoni, M. Cavenago, G. Chitarin, H. de Esch, A. D. Lorenzi, N. Fonnesu, G. Gambetta, R. Hemsworth, M. Kashiwagi, N. Marconato, D. Marcuzzi, N. Pilan, E. Sartori, G. Serianni, M. Singh, P. Sonato, E. Spada, V. Toigo, P. Veltri, and P. Zaccaria, Nuclear Fusion **56**, 016015 (2015).

[36] M. Singh and H. de Esch, Review of Scientific Instruments **81**, 013305 (2010), https://doi.org/10.1063/1.3271535.

[37] *Rare earth permanent magnets; VACODYM VACOMAX*, VACUUMSCHMELZE GmbH & Co. KG, pd002 ed. (2014).

[38] P. Agostinetti, V. Antoni, M. Cavenago, G. Chitarin, N. Marconato, D. Marcuzzi, N. Pilan, G. Serianni, P. Sonato, P. Veltri, and P. Zaccaria, Nuclear Fusion **51**, 063004 (2011).

[39] W. Kraus, L. Schiesko, F. Bonomo, U. Fantz, B. Heinemann, and A. Hurlbatt, AIP Conference Proceedings **2052**, 040004 (2018), https://aip.scitation.org/doi/pdf/10.1063/1.5083738.

[40] G. Chitarin, P. Agostinetti, D. Aprile, N. Marconato, and P. Veltri, AIP Conference Proceedings **1655**, 040008 (2015), https://aip.scitation.org/doi/pdf/10.1063/1.4916450.